Eur. Phys. J. Plus (2024) 139:432
https://doi.org/10.1140/epjp/s13360-024-05208-w

THE EUROPEAN PHYSICAL JOURNAL PLUS

Review

Shutdown dose rate experiment at JET during DTE2

N. Fonnesu[1,a], S. Loreti[1], R. Villari[1], D. Flammini[1], G. Mariano[1], P. Batistoni[1], A. Colangeli[1], F. Moro[1], A. Previti[1], A. Klix[2], JET Contributors

[1] Nuclear Department, ENEA, Via E. Fermi 45, 00044 Frascati, Rome, Italy
[2] Karlsruhe Institute of Technology, 76344 Eggenstein-Leopoldshafen, Karlsruhe, Germany
[3] EUROfusion Consortium, JET, Culham Science Centre, Abingdon OX14 3DB, UK

Received: 15 December 2023 / Accepted: 21 April 2024

Abstract The EUROfusion activities on the technological exploitation of deuterium–tritium (DT) operation at JET (started within the work package JET3 and continued under PrIO) were established to maximize the scientific and technological return of DTE2 campaign occurred in the second part of 2021. In particular, the aim of the NEXP sub-project was to take advantage of the expected significant neutron production during DTE2 to validate the numerical tools used for neutron streaming and shutdown dose rate (SDR) calculation for ITER through the comparison between numerical predictions and measurements. In the frame of SDR activity, a dosimetry system to measure the dose rate and based on some ionization chambers (ICs) was installed in the torus hall and upgraded both hardware and software since 2015 by exploiting the previous DD and TT campaigns. Two spherical 1-L air-vented ICs had been installed in some ex-vessel positions close to the horizontal ports of the tokamak in octants 1 and 2 and a third IC, suitable for higher dose rates, was then added in octant 1. As for SDR calculation, numerical tools employed rely on MCNP code for radiation transport and in this regard the MCNP model has been updated to include the last detector installed in octant 1. The present work is dedicated to the analysis of dose rate measurements carried out during DTE2 in the inter-pulse periods and at the shutdown. Influence quantities and error sources are analyzed to calculate the dose rate from raw signal and experimental uncertainty. Some experimental points are chosen and employed for a preliminary comparison with numerical predictions obtained from three-dimensional simulations with Advanced D1S tool. The results are presented and discussed with the major objective to contribute to the optimization of the planned SDR code validation.

1 Introduction

Since the first high fusion power deuterium–tritium (DT) campaign at JET in 1997 (DTE1), significant enhancements have been applied to the tokamak in preparation of the subsequent DTE2 campaign occurred at the end of 2021 [1]. Over the years, the nuclear technology program at JET has been carried out mainly with the aim of maximizing the scientific return from the high neutron budget of DTE2 and it has benefited from the relevant neutron yield of deuterium–deuterium (DD) campaigns occurred in 2016, 2019, 2020 and from lessons learned during less intense tritium–tritium (TT) campaigns.

The technological exploitation of DTE2 campaign at JET, started with EUROfusion work package (WP) JET3 [2, 3] and continued under WP PrIO (Preparation of ITER operation) through NEXP subproject [4, 5], intended to take advantage of the significant neutron production to validate numerical tools used for the assessment of neutron streaming and shutdown dose rate (SDR) under operating conditions of relevance for ITER. In particular, the assessment of dose rate due to the decay gamma radiation field produced by neutron activation of surrounding materials is of paramount importance in ITER for planning its operation and maintenance in compliance with radiation exposure limits of workers. It follows that the accuracy of the numerical tools employed for SDR need proper assessment. Two methodologies have been followed for the development of SDR computer tools, which couple a radiation transport code (e.g., MCNP5 [6]) and an inventory code for assessing neutron activation of materials (e.g., FISPACT [7]), i.e., the so called Direct one step method (D1S) [8, 9] which brought, among the others, to Advanced D1S [10, 11], and the so called Rigorous 2-step (R2S) approach [12].

In this regard, a dosimetry system to measure the dose rate in the inter-pulse intervals across the experimental campaigns and at the shutdown, based on some ionization chambers (ICs), was installed in the torus hall and upgraded both hardware and software since 2015 by exploiting the DD and TT campaigns [13–16], since the 2016 DD campaign (C36).

See the author list of "Overview of T and D-T results in JET with ITER-like wall" by CF Maggi et al. to be published in Nuclear Fusion Special Issue: Overview and Summary Papers from the 29th Fusion Energy Conference (London, UK, 16-21 October 2023).

[a] e-mail: nicola.fonnesu@enea.it (corresponding author)

Published online: 21 May 2024

Table 1 JET campaigns since 2016 (neutron yields are calculated from the JET neutron monitor KN1 data)

JET campaign	Start date	End date	Total N yield	Max N yield per pulse
C36a (DD)	04/01/2016	27/06/2016	7.63E+18	5.01 E+16
C36b (DD)	10/10/2016	15/11/2016	1.13E+19	1.26E+17
C38a (DD)	03/06/2019	20/12/2019	3.69E+19	1.47E+17
C38b (DD)	17/02/2020	23/03/2020	1.49E+19	2.14E+17
C38c (DD)	06/07/2020	26/09/2020	1.66E+19	1.92E+17
C39T (TT)	07/12/2020	18/12/2020	6.08E+15	1.60E+15
C40 (TT)	04/01/2021	31/07/2021	8.52E+18	1.46E+17
C41 (DT, a.k.a. DTE2)	**08/08/2021**	**21/12/2021**	**8.48E+20**	**2.09E+19**
C40 (T-Post DT)	17/01/2022	04/03/2022	2.48E+18	2.13E+17
C42 (D – T removal)	07/03/2022	26/08/2022	8.25E+18	1.80E+17
C43 (Helium)	01/09/2022	07/11/2022	9.74E+14	3.46E+14
C44 (Deuterium)	08/11/2022	16/12/2022	4.02E+18	1.01E+17

As a reference, Table 1 lists the JET experimental campaigns since 2016, including total and maximum neutron yield per pulse (neutron yields are elaborated by the authors from the JET neutron monitor KN1 data, DTE2 data are in bold).

The DTE2 campaign, occurred in the period August-December 2021, achieved a new record in terms of energy produced in a single fusion plasma pulse (i.e., 59 MJ, more than doubling the previous one obtained during DTE1) and addressed several important physics and technological open points. From the nuclear technology standpoint, the relevance of this campaign is in the significant total 14-MeV neutron yield of about 8.5×10^{20} reached in an ITER-relevant machine as JET, with a maximum daily yield of about 1.0×10^{20} on the last day of the campaign.

For the reasons mentioned above, the experimental data collected by ionization chambers (and other detectors within the same work program) during DTE2 represent a unique opportunity to refine and validate the numerical tools for ITER nuclear analysis, through the comparison between numerical predictions and measurements (C/E). Measurements and SDR predictions are compared in terms of air kerma rate, which is equivalent to absorbed dose rate in air as long as the condition of charged particle equilibrium holds [17].

The present work is dedicated to the measurement of SDR across DTE2 in the inter-pulse intervals and at the shutdown. Influence quantities affecting SDR measurements and error sources are analyzed to calculate the dose rate from raw signal and experimental uncertainty. Some experimental data are then selected for a preliminary comparison with numerical predictions obtained by Advanced D1S, based on MCNP5 and FISPACT codes. The input preparation phase mainly consisted in the update of the MCNP geometry model of JET octant 1 (the third detector, i.e., the small IC in octant 1 was included in it, together with a new set of activation foils located on the same shelf) and the neutron irradiation history for FISPACT made from the neutron emissivity data from KN1 through a dedicated computer routine. Results are presented and discussed with the major objective to contribute to the optimization of the planned benchmark of the main SDR tools employed in neutronics for fusion.

The manuscript is organized as follows: Sect. 2 gives an overview of the experimental setup (both hardware and software); Sect. 3 is dedicated to the measurements (from the calibration of dosimeters and raw signal elaboration to the uncertainty analysis); Sect. 4 reports about preliminary numerical predictions, including the input preparation for the radiation transport and neutron activation simulations and the comparison with SDR measurement at some selected cooling times. Conclusions and future work are given in Sect. 5.

2 Experimental setup

The measuring equipment selected for the SDR experiment consists of three active dosimeters calibrated in terms of air kerma and based on three air-vented spherical ionization chambers (ICs) designed for radiation protection. Two of the three ICs are 140 mm diameter, with a sensitive volume of 1000 cm^3, model 32,002 produced by PTW [17]. They are installed on the side port of octant 1 close to the Radial Neutron Camera (labeled IC Oct1 big) and in octant 2 on top of the ITER-like Antenna (labeled IC Oct2 big). The third IC (labeled IC Oct1 small) is 44 mm diameter, sensitive volume of 30 cm^3, PTW model 32,005 [18] located in octant 1 on the same shelf as IC Oct1 big and with a lower response (about 1/40 w.r.t. to the latter) and for this more suitable for higher dose rate level (compared to the intensity measured during DD campaigns) as expected during DTE2 campaign. Such ICs were selected for their characteristics of excellent reproducibility, long-term stability of the sensitive volume and flat energy response in terms of air kerma, which is essential in this application, considering the complexity of the gamma radiation field at JET as well as low neutron activation. The spherical construction ensures a nearly uniform response to gamma radiation from every direction.

The layout of the experimental assembly and data handling is shown in Fig. 1. The ICs are operated in current mode and the ionization current (produced by the interaction of air with gamma radiation field) is analyzed by three suitable electrometers, one

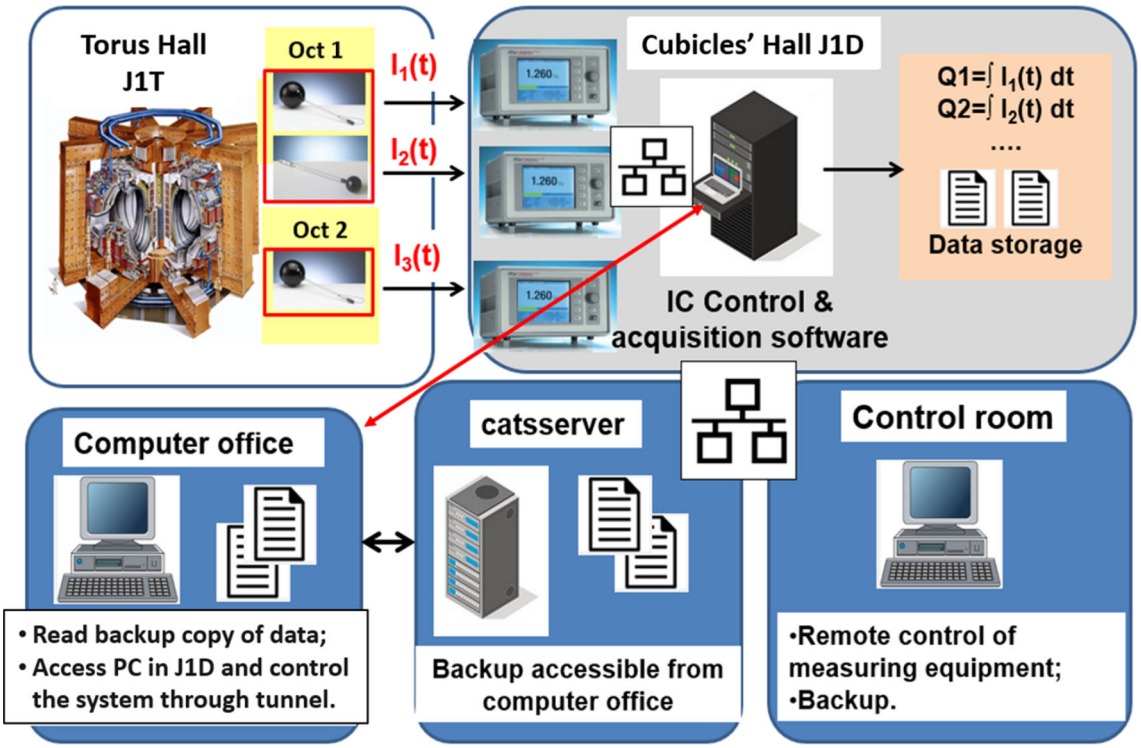

Fig. 1 Layout of the experimental assembly and data handling

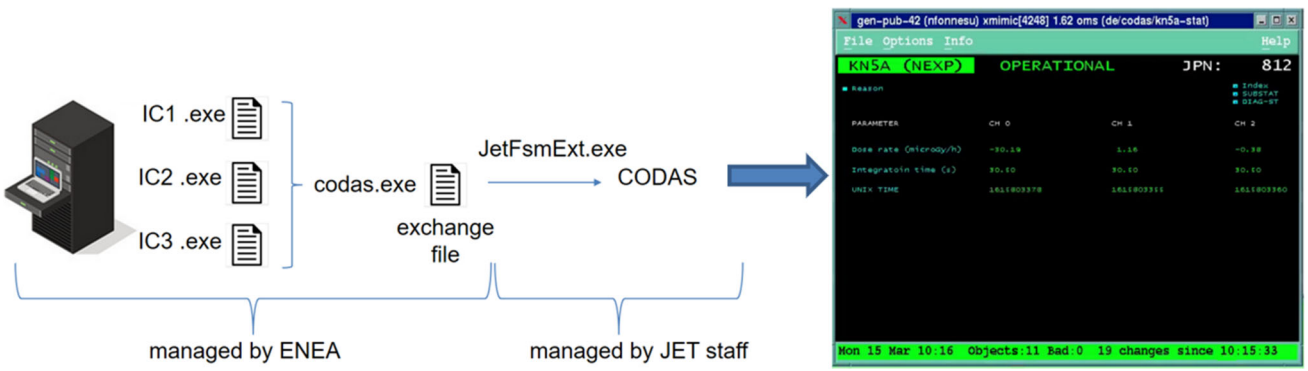

Fig. 2 Scheme of the software for dosimeter control, data acquisition and data sharing with CODAS

for each dosimeter. The electrometers, model PTW UNIDOS [18], are equipped with an Ethernet interface employed to connect them to the computer. Both are located in the cubicles'hall (J1D). A low noise connection between IC in the torus hall (J1T) and electrometer is made through triaxial cables, approximately 100 m long, designed for precise current measurements (down to fA) and with a low leakage caused by irradiation. They provide insulated potentials for the measuring signal, the guard electrode, and high voltage to ICs (400 V).

The PC in J1D controls the measuring assembly and data acquisition by means of a piece of software developed by ENEA for the specific application. Such a piece of software allows the remote control of electrometer through a TCP/IP connection, data handling and storage and it manages a single dosimeter. It gives also a complete instrument reading and some information related to the communication with the electrometer. The recorded data is sent once a day to the JET server named catsserver as backup. The system is also manageable from remote through network tunneling.

The scheme in Fig. 2 shows how data is shared with CODAS (Control and Data Acquisition System). IC1.exe, IC2.exe and IC3.exe execute the same piece of software earlier mentioned, one for each detector. A fourth piece of software (codas.exe) writes the dose rate data into an exchange file accessible to JetFsmExt.exe, i.e., the application provided by JET CODAS (Control and Data Acquisition System) that allows non-integrated software to access the JetFsm infrastructure in a file-based manner. A real-time copy of SDR data is sent consistently to CODAS via HTTP protocol and made available in the Continuous Data Recording System (CGRT) on Solaris data store. A dedicated mimic is also available as virtual instrument reading as shown in the same figure.

Table 2 Air kerma calibration coefficient of the three dosimeters

IC	Radiation quality	N_{kair} (Gy/C)
IC Oct1 small	X-ray tube (40,150,300 keV)	1.112×10^6 ($U = 3.73\%$)
	Am (59 keV)	
	Cs (662 keV)	
	Co (1253 keV)	
IC Oct1 big	X-ray tube (40,150,300 keV)	2.451×10^4 ($U = 4.08\%$)
	Am (59 keV)	
	Cs (662 keV)	
	Co (1253 keV)	
IC Oct2 big	Co (1253 keV)	2.504×10^4 ($U = 2.50\%$)

3 Measurements

To obtain air kerma rate, ionization current I(t) measured by electrometers is integrated over a time interval Δt for calculating the collected charge $Q(\Delta t)$. The average value of the charge collected in the ionization chamber per unit of time ($Q/\Delta t$) is the raw measurement (M_{raw}). In order to have a good statistics for the calculation of the average value of the charge collected per unit of time, Δt was set equal to 30 s during the campaign and, contrary to what was done in the past (when we used to increase time interval up to 600 s at the end of campaigns), it was kept the same also after the end of DTE2 as the ionization current was sufficiently high to limit statistical fluctuation in the measurement of $Q/\Delta t$.

Air kerma rate is calculated following the formalism of dosimetric protocols [19, 20] through the formula below (1), where ${N_K}^{cal}$ is the calibration coefficient to convert the corrected instrument reading M_{corr} (see Sect. 3.2) into air kerma rate. $k_{Q,Q0}$ is a factor to account for the difference in beam qualities during calibration (Q_0) with respect to the measured radiation field (Q).

$$\dot{K}_{air} = N_K^{cal} \cdot M_{corr} \cdot k_{Q,Q0} \tag{1}$$

Considering the peculiarity of SDR experiment, where a radiation field with a broad energy spectrum is measured (while protocols essentially refer to mono-energetic beams), $k_{Q,Q0}$ is not directly applicable. The energy dependency of the dosimeter response was assessed in a different manner as explained in the following.

3.1 Calibration

The two dosimetry systems in octant 1 were calibrated at ENEA-INMRI [21] in terms of air kerma, using the selected X and gamma reference beam qualities at low doses (the range of interest is<40 mSv/h) and according to ISO guidelines [22]. Radiation qualities employed were filtered X-rays produced with an accelerated electron beam (at 40, 150, 300 keV), and gamma-emitters Am241, Cs137, and Co60. A calibration certificate was also provided by the manufacturer (PTW) for Co60 for all the dosimeters and the calibration of the one in octant 2 relies only on this.

Table 2 reports radiation qualities employed for the calibrations and average photon energy. The calibration coefficients are reported together with expanded measurement uncertainty U (coverage factor$k = 2$, which gives a level of confidence of approximately 95%).

As earlier mentioned, the gamma radiation field at JET has a complex and broad-energy spectrum and the energy dependence of the dosimeters must be accounted. The calibration coefficient of dosimeters in octant 1 being the weighted average of the values measured at the different radiation qualities [13] (weights are the inverse square of the associated uncertainties) within the energy range 40–1253 keV accounts also for the energy dependency of the dosimeter response, while the calibration of dosimeter in octant 2 does not include energy dependency as it relies on a single radiation quality. This will be accounted in the uncertainty budget of such dosimeter by including the energy dependency as calculated by the manufacturer as a separate source of uncertainty.

3.2 Influence quantities

The assessment of influence quantities affecting dosimetric measurements and the mitigation of their effects to a negligible level is based on some codes of practice (e.g., see [19, 20]). The instrument reading indicated asM_{raw} is the raw measurement to be corrected, which in our case is the charge collected per unit of time ($Q/\Delta t$). A number of correction factors applies to this value to account for variations from the reference calibration conditions and to limit the effect of influence quantities. The following correction factors are considered for the calculation of the corrected instrument reading M_{corr}:

$$M_{corr} = M_{raw} \cdot k_{TP} \cdot k_h \cdot k_{sat} \cdot k_{stab} \cdot k_{lin} \cdot k_{leak} \cdot k_{rot} \cdot k_{oxygen} \tag{2}$$

These factors are discussed in the following. Uncertainty related to the application of such corrections, is neglected if its (expanded) value is < 0.1%.

3.2.1 Air temperature and pressure (k_{TP})

ICs are air-vented and therefore sensitive to the air condition in the torus hall where they are located. The ionization current produced in the spherical sensitive volume of ICs is proportional to the mass of air and, to account for air density variation with respect to reference standard conditions during calibration (i.e., temperature $T_0 = 293.15$ K and pressure $P_0 = 1013$ hPa), the correction factor k_{TP} is applied. Assuming that ideal gas law holds for the ambient air, it takes the following form:

$$k_{\mathrm{TP}} = \frac{P_0}{T_0}\frac{T_{\mathrm{IC}}}{P_{\mathrm{IC}}} \tag{3}$$

The role of relative humidity in air density variation is considered negligible. The calculation of k_{TP} has required monitoring temperature (T_{IC}) and pressure (P_{IC}) during the experimental campaign. No dedicated instruments have been provided for measuring air temperature and pressure near the two dosimeters in the JET torus hall and the only measurement of temperature available for air density correction (T_{HVAC}) comes from the ventilation system (HVAC) of the torus hall, whose diagnostics are integrated in CODAS system. Considering the proximity of ICs to the tokamak, whose in-vessel components during operations are warmed up to about 300 °C, and that the thermometer of HVAC system is located far from it, the temperature of air inside IC cavity is estimated as T_{HVAC} + 5 K, within a uniform distribution limited by $T_{\mathrm{IC}} \pm 5$ K. This means a relative expanded uncertainty for T_{IC} of 1.7%, considering the range 292–303 K. Air pressure P_{IC} comes from a baratron close to the High Voltage tower of neutral injectors (NBIs) in octant 8. The expanded uncertainty related to this estimation is conservatively evaluated as ± 10 hPa (1.0% of P_{IC}) with a uniform distribution. Air temperature and pressure are recorded in the CODAS CGRT data store every 30 s and 180 s, respectively, and the values at the times of dose measurement are calculated with linear interpolation. Errors associated to the assumption of linear variation of these quantities in such time intervals are considered negligible. The correction due to air density variation during measurements is in the range 0.97–1.07.

3.2.2 Humidity (k_h)

Humidity influences air density, the average energy for producing an ion pair and the mass stopping power for electrons, which in turn affect the instrument reading [23]. The variation of the three quantities usually compensates each other so that the overall effect is smaller. The error introduced by ignoring variations in relative humidity (RH) in the range 20 to 80%, is within ± 0.15% of the reading [20]. RH is calculated from dew temperature (T_{dew}) records available from CODAS (HVAC system), by applying the Magnus formula [24]. Accounting for the uncertainties introduced in the calculation of relative humidity by the Magnus formula (about 0.1%) and even more by the T_{IC} value (about 10%), RH is in the range 17–65%, and the above-mentioned error of ± 0.15% is reasonably applicable. For this, no correction is applied to M_{raw}, i.e., $k_{\mathrm{h}} = 1$ and the (expanded) uncertainty is ± 0.15% (uniform distribution).

3.2.3 Ion recombination (k_{sat})

A fraction of charges produced by the radiation field recombines before being collected and measured thus inducing a loss of signal. Since during the calibration of dosimeters at ENEA-INMRI [21] the instrument reading was corrected for considering ion recombination, which means that the calibration coefficient ${N_K}^{\mathrm{cal}}$ applies to the instrument reading incremented for the recombination loss, the same correction coefficient is applied before converting the signal into air-kerma. Such correction is about 0.1–0.2% and the uncertainty on applying this correction is neglected.

3.2.4 Stability (k_{stab}), linearity (k_{lin}), leakage current (k_{leak})

The time stability measured by the variation of the dosimeter response to the same identical radiation field in the course of time is taken as ± 1% for the ionization chambers and ± 0.1% for the electrometer [18]. Such uncertainties are from manual and supported by the results of the calibration check performed in November 2019 both in octants 1 and 2. So, to account for the non-perfect long-term stability, no correction is applied ($k_{\mathrm{stab}} = 1$) and the mentioned uncertainties with uniform distribution accounted.

No correction is applied also for the non-perfect linearity of the instrument ($k_{\mathrm{lin}} = 1$) and this, according to the manufacturer, brings to a maximum error of ± 0.25%, considered in the uncertainty budget.

As for the leakage current due to the high voltage applied inside the ionization chambers and in the cable, it is usually < 0.1% of the signal $I(t)$. Before starting dose rate measurements, the average value of ionization current due to the background radiation in the torus hall (I_{bkg}), which also includes leakage current, has been measured and then subtracted from $I(t)$ during SDR measurements. For this reason, under the hypothesis of constant leakage current, such effect has already been removed from M_{raw} and no correction factor is needed. Uncertainty on this correction is reasonably supposed to be < 0.1% and it has been neglected.

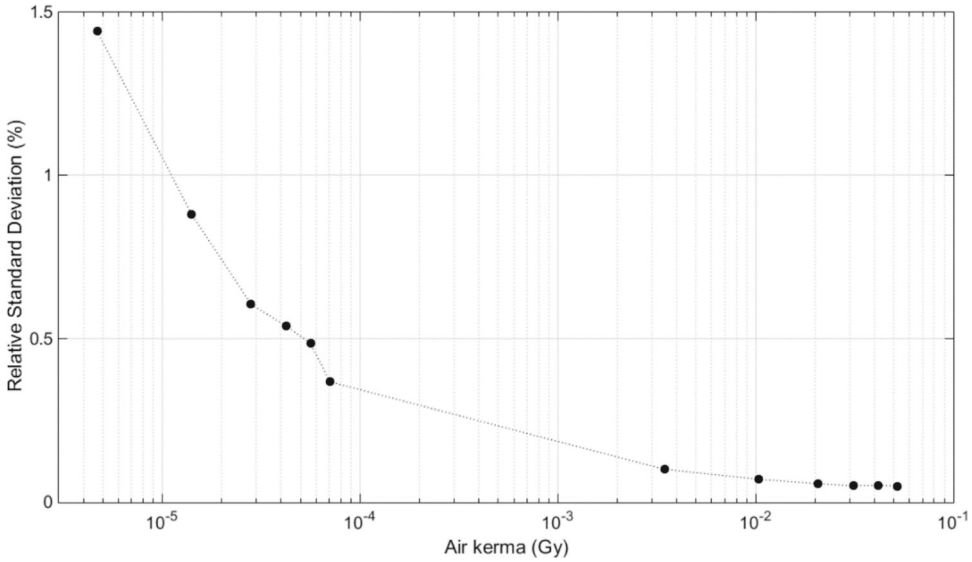

Fig. 3 Relative standard deviation of the signal (% of the mean value) as a function of the air kerma as oxygen concentration in the air inside the glass box varies from 14 to 21%

3.2.5 Direction of radiation field (k_{rot})

The reference radiation field under which dosimeters were calibrated is perpendicular to their longitudinal axis while at JET they are exposed to a complex gamma radiation field made of several gamma sources and impinging dosimeters from many directions. The experimental assessment of a correction factor for the field geometry would be extremely difficult and, in lack of its measurement, no correction is applied ($k_{\mathrm{rot}} = 1$) and the variation of the dosimeter response due to the angular dependence is accounted in the uncertainty budget. Such dependence is $\pm 3\%$ (for the small IC) and $\pm 5\%$ (for the big ICs) for tilting the longitudinal axis with respect to the perpendicular field and $\pm 0.5\%$ for rotation around the same axis for all ICs.

3.2.6 Oxygen concentration into the air (k_{oxygen})

When JET is fueled with tritium, as a preventative measure for fire suppression, the concentration of oxygen (O_2) in the air inside the torus hall is reduced to about 15% by increasing the content of nitrogen (N_2). This has an impact on the charge creation due to the ionization of air and their collection inside the detectors. As the variation of air composition in ICs is uncommon and no studies were found in the literature, a dedicated experiment was performed at ENEA Frascati with the big IC now installed at JET in octant 2, as reported in [16] and here recalled for the sake of completeness of the analysis. An oxygen-deficient atmosphere was created inside a glass box by inflating N_2. In the same box the IC and a gamma source were installed. The O_2 concentration was varied at a rate sufficiently slow (i.e., about 1% of variation in 30 min) with respect to the stabilization time of the IC (about 15 min), to guarantee an equilibrium condition before reading the signal. Correction for air pressure and temperature inside the box were applied to exclude their influence. Co60 and AmBe gamma sources were employed to expose the IC to air kerma rate of about 5 μGy/h and 3.4 mGy/h, respectively. The sensitivity of IC was measured as a function of the O_2 concentration and of the dose cumulated by means of the two radiation sources and by varying the integration time Δt from 300 to 4500 s. The main outcome of the experiment is shown in Fig. 3, where the signal variation (represented by the relative standard deviation of the charge) measured by the dosimeter as a function of the air kerma and, at each air kerma value, as the O_2 concentration varies from 14 to 21%, is plotted. The influence of O_2 concentration on the signal variation is $\leq 1.4\%$ for air kerma > 5 mGy.

In the torus hall the O_2 concentration is monitored by 4 sensors around the tokamak. It has been decided not to apply an online correction based on these measurements (i.e., $K_{\mathrm{oxygen}} = 1$) but only to check the limits of oxygen variation and then to apply the uncertainty of 1.4%, applicable as long as the air kerma > 5 mGy.

3.3 Experimental uncertainty and PDF

The overall uncertainty on SDR measurements is obtained by applying the error propagation formula to the expression of air kerma rate, according to the ISO GUM recommendations for the calculation of measurement uncertainty [25]. Considering the simple multiplicative form of the expression of air kerma rate and the absence of correlation of input quantities, the relative uncertainty of air kerma rate can be written as the root of the sum of squared relative standard deviation of the input quantities:

$$\frac{u_{\dot{K}\mathrm{air}}}{\dot{K}_{\mathrm{air}}} = \sqrt{\sum_{i=1}^{N} \frac{u^2(x_i)}{x_i^2}} \tag{4}$$

Table 3 Sources of uncertainty and overall experimental uncertainty (in bold) in the measurement of air kerma rate with dosimeters based on IC Oct 1 small, IC Oct 1 big, IC Oct2 big

Source of uncertainty	Correction factor	Expanded uncertainty (%)	PDF	Type of uncertainty	Confidence level %	Coverage factor	$u(x_i)/xi$ (%)
Temperature	K_{TP}	1.70	Rect	A	100	1.73	0.98
Pressure	K_{TP}	1.00	Rect	A	100	1.73	0.58
Humidity	K_h	0.15	Rect	B	100	1.73	0.09
Ion recombination	K_{sat}	Neglected	–	–	–	–	–
Stability (IC)	K_{stab}	1.00	Rect	B	100	1.73	0.58
Stability (electrometer)	K_{stab}	0.10	Rect	B	100	1.73	0.06
Linearity	K_{lin}	0.25	Rect	B	100	1.73	0.14
Leakage current	K_{leak}	Neglected	–	–	–	–	–
Tilting	K_{rot}	3.00/5.00/5.00	Rect	B	100	1.73	1.73/2.89/2.89
Rotation	K_{rot}	0.50	Rect	B	100	1.73	0.29
Oxygen	K_{oxygen}	1.40	Rect	B	100	1.73	0.81
Resolution (Q)	–	0.50	Rect	B	100	1.73	0.29
Repeatability	–	0.25	Norm	B	68	1.00	0.25
Energy dependency	–	– /– / 4.00	Rect	B	100	1.73	– /– / 2.31
Calibration factor	N_{kcal}	3.73/4.08/2.50	Norm	A	95	2.00	1.87/2.04/1.25
Experimental Uncertainty					**66/64/66**	**1.00**	**3.0/3.9/4.2**

where u_{Kair} is the variance of air kerma rate and x_i is the generic input quantity with variance $u^2(x_i)$. Sources of uncertainty in the measurement of air kerma rate with dosimeters based on IC Oct 1 small, IC Oct 1 big, IC Oct2 big are listed in Table 3, including probability distribution functions (PDF), type of uncertainty (type A is based on a statistical analysis of repeated observations, type B includes essentially scientific judgment and manufacturer's specifications), confidence level, coverage factor, relative standard deviation. In addition to uncertainties on the application of correction factors to the instrument reading as described in Sect. 3.2, digital resolution of the electrometer, repeatability, energy dependency (applied only to dosimeter in octant 2 as for the dosimenters in octant 1 the energy dependency was measured considered in their calibration explained in Sect. 3.1) and uncertainty on the calibration are also listed and included in the uncertainty budget. The resulting experimental uncertainty is given as well (in bold, last row).

The experimental uncertainty of air kerma rate (expressed as the relative standard deviation) measured with the three dosimeters based on IC Oct1 small, IC Oct1 big and IC Oct2 big, is 3.0%, 3.9% and 4.2%, respectively. The PDF of air kerma rate was assessed through Monte Carlo sampling with a dedicated computer routine. Random number generators implemented are compliant with the guidelines for propagation of distributions included in the supplement of the ISO GUM [26] and are taken from [27]. Despite some relevant sources of uncertainty are not Gaussian, in all the three cases the resulting PDF is close to a Gaussian, the confidence probability associated to the standard deviation being equal to 66, 64 and 66%, respectively.

The largest source of uncertainty is the one associated to the radiation field direction (tilting angle). Calibration factor is the second most relevant for dosimeters in octant 1, while in octant 2, energy dependency has a more relevant weight than calibration in determining the overall experimental uncertainty.

3.4 SDR measurement during DTE2

DTE2 was carried out at JET from the beginning of August to December 21st, 2021, with the highest performance in terms of sustained fusion energy and consequent neutron production occurred in the last day of the campaign, when more than 1×10^{20} neutrons, i.e., 12% of the total neutron budget of the campaign, were produced. In the same day, the highest neutron yield per pulse ($>2 \times 10^{19}$) was achieved during two plasma discharges.

Air kerma rate was measured in octants 1 and 2 across the campaign (inter-pulse periods) and after shutdown uninterruptedly, exception done for the IC in octant 2 which, after the first week of December, was turned off for some technical issues unrelated to the dosimeter itself but to the cubicle housing the electrometers. It was restarted after DTE2 in the second part of January 2022. Measurements for the periods November 2021 and December 2021-January 2022 are shown in the lower plots of Fig. 4a, b Green, blue and red lines are the air kerma rate as measured by IC Oct1 small, IC Oct1 big and IC Oct2 big, respectively, while the circles represent the calculated dosimeters' response for some selected cooling times, as discussed in Sect. 4. The neutron yield of each pulse is shown in the upper plots of the same figures, calculated as the time integral of the neutron emissivity measured by the JET

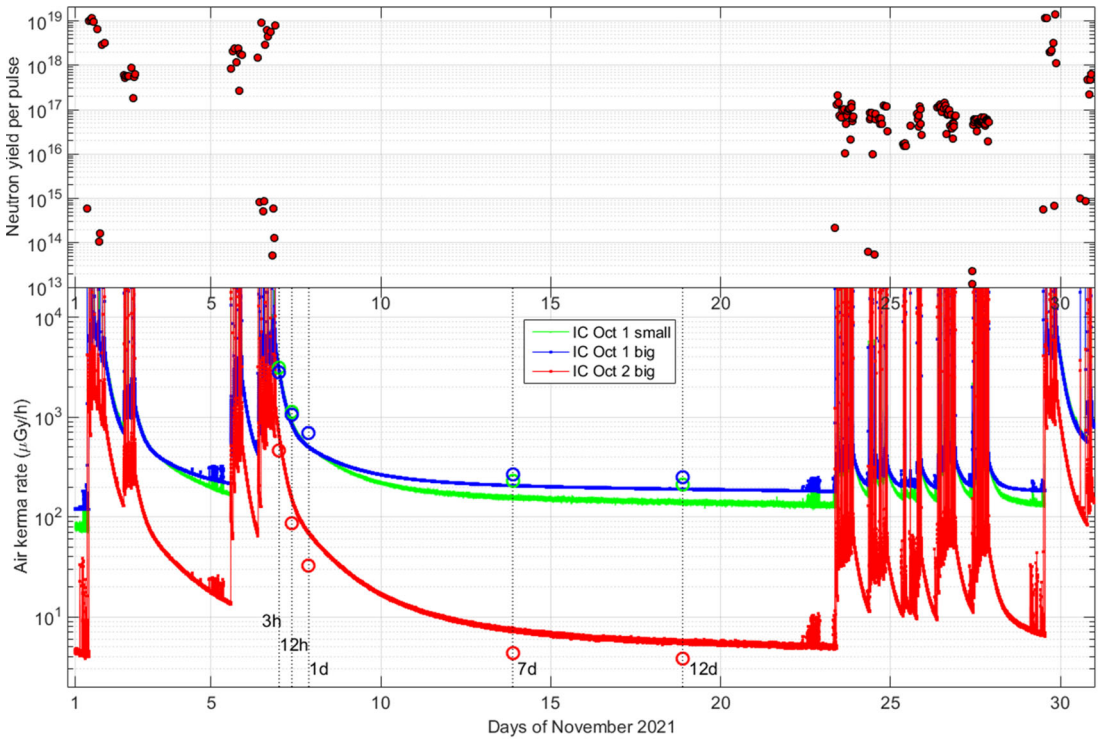

(a)

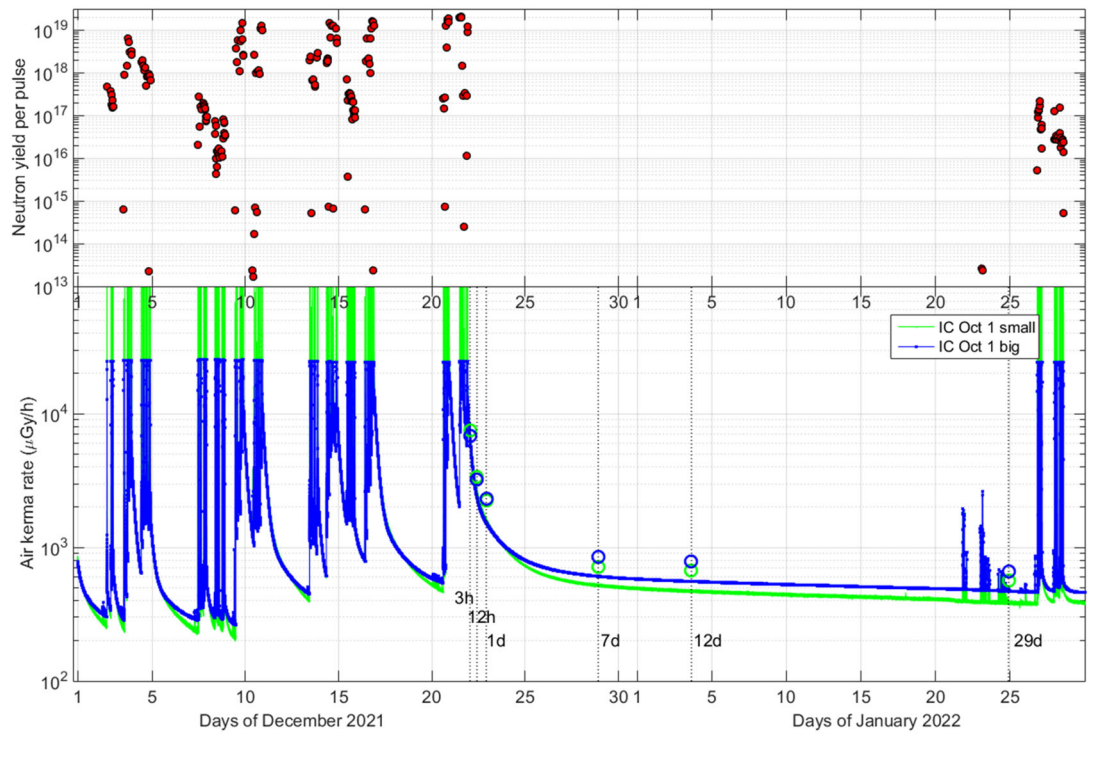

(b)

Fig. 4 Neutron yield per pulse (top) and air kerma rate in μGy/h (bottom) in November 2021 (a) and December 2021- January 2023 (b) during DTE2 campaign at JET and after shutdown as measured by the three dosimeters in octant 1 (IC Oct1 small, IC Oct1 big) and octant 2 (IC Oct2 big). Circles represent the preliminary results of Advanced D1S (cf. Section 4) for the selected cooling times as indicated by the labels

neutron monitor KN1. During the neutron emission the dosimeters reach the electric current limit of the selected measuring range. This does not represent a concern as dosimeters are not calibrated to measure the dose due to neutrons and there is not interest in following the signal peak produced during the plasma discharges which also represent a transient for the ICs, their stabilization time

Table 4 Some experimental days of interest for SDR tool benchmark and measurement range after the last pulse of the day

Day	Cooling time range	SDR range		
		Octant 1		Octant 2
		IC Oct1 small	IC Oct1 big	IC Oct2 big
October 2nd	3 h–5 days	1 mGy/h–95 μGy/h	1 mGy/h–139 μGy/h	209–6 μGy/h
November 6th	3 h–14 days	3 mGy/h–137 μGy/h	3 mGy/h–185 μGy/h	658–5 μGy/h
December 21st	3 h–1 month	8 mGy/h–387 μGy/h	7 mGy/h–470 μGy/h	–

being much longer than neutron emission. SDR measurements considered in this experiment must be sufficiently far in time from plasma pulses to avoid the influence of activation of the air inside the chamber on the measurement of the radiation field induced by neutron activation.

In octant 1, the big IC measures a higher dose rate compared to the smaller one and this can be explained as the first is more exposed to the opening of equatorial port so to the radiation field from the inner component of the plasma chamber.

As the scope of these measurements is to provide experimental data for code benchmarking of SDR tool, methodologies and nuclear data employed for assessing SDR in ITER, the range of dose measured is of paramount relevance. In particular, the intervals measured in octant 1, i.e., about 100 μGy/h to 20 mGy/h, and in octant 2, i.e., about 4 μGy/h to about 1 mGy/h, are relevant both for ITER interspaces and port cells SDR analyses.

From the set of measurements produced, some specific points are being selected for the benchmark campaign. Some days of interest are listed in Table 4, including the cooling time range considered after the last pulse of the day and the dose rate range measured, both in octant 1 and 2. Several measurement points from 3 h to 5 days after last pulse of October 2nd are available. Dose rate range in octant 1 is from 1 mGy/h after 3 h, to about 0.1 mGy/h after 5 days. In octant 2 the range is from 0.2 mGy/h (after 3 h) to 6 μGy/h (after 5 days). The long inter-pulse period, about 14 days, after the last week of November is relevant as well. In particular, after plasma pulses of November 6th and before the next experimental day, dose rate ranges in octant 1 from 3 mGy/h (after 3 h) to 0.14 mGy/h (after 14 days). Then, the final shutdown after the high fusion power pulses of the last day of the campaign, December 21st, offers interesting measurement points for the benchmark. Dose rate varies approximately from 8 mGy/h (3 h after shutdown) to 0.5 mGy/h (after 14 days) in octant 1. After about 1 month, dose rate level in octant 1 is still considerably high as about 0.4 mGy/h.

4 Input preparation and some preliminary numerical predictions

Advanced D1S is one of the SDR tools involved in the benchmark against DTE2 measurements. Based on the D1S approach and developed by ENEA [10, 11], it relies on a single computer simulation which couples neutron and decay gamma transport. It is based on a modified version of the MCNP5 with specially tailored nuclear cross-section data for transport and FISPACT for temporal behaviour. It has been validated through previous measurements at JET [11] and comparison with R2S codes and it has also been extensively used for the analysis of other relevant fusion projects (ITER, DEMO and DTT). For the present benchmark, an improved version, i.e., Advanced-D1S Dynamic [28, 29], with further features aimed at extending applications and at improving its versatility was employed. Further details are available in [29].

The main input data required by SDR tools for the DTE2 benchmark campaign, i.e., the MCNP model and the JET neutron irradiation history for the inventory code, were updated and produced, respectively, as detailed in the following.

Some preliminary SDR predictions by Advanced D1S have been then compared against experimental measurements with the major objective to contribute to the selection of relevant measurement points for the benchmark of the main SDR tools employed for nuclear analyzes and to test as well the inputs for MCNP and FISPACT.

The neutron transport simulations were performed with MCNP5 using the 45° geometrical models of octants 1 and 2 [30]. Material description includes impurities based on available chemical certificates and the reflective boundary condition on the lateral sides of the models is applied to simulate full 3D transport. FENDL 3.1d [31] nuclear libraries are used. The model of octant 1 has been updated to include the new configuration of the shelf housing the two ICs and a new set of activation foils. A 3D CAD drawing (step file) was created from a 3D scan of the shelf. The inner structure of detectors, known from technical drawings made available by the manufacturer PTW, was implemented in the CAD file with the use of Space Claim [32]. The CAD was then defeatured in the same modeling environment and then converted into MCNP geometry with Super MC [33] and integrated into the overall MCNP model of JET octant 1. In Fig. 5, the geometry model of octant 1 is shown with the magnification of the shelf housing the detectors, as after defeaturing and removing irrelevant details. In between the two detectors, the activation foil holder for passive measurement of neutron fluence [34] was placed.

As for the activation calculation, for past DD experiments, the entire JET neutron irradiation history was used to calculate the activation level of the components of the machine at the time of the experiment. In case of DTE2, the contribution to material activation

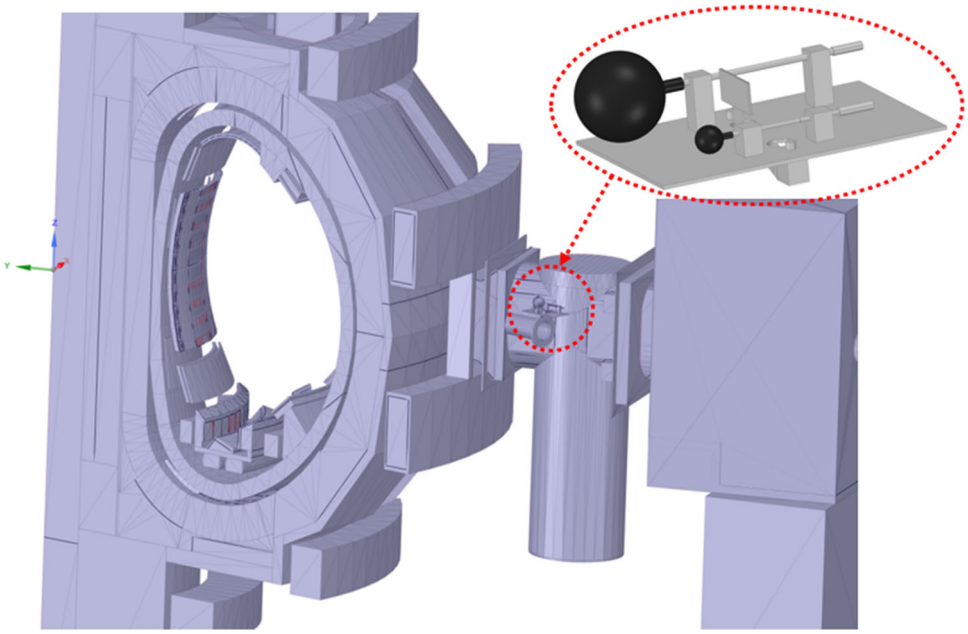

Fig. 5 Geometry model of JET octant 1 as updated for DTE2 campaign

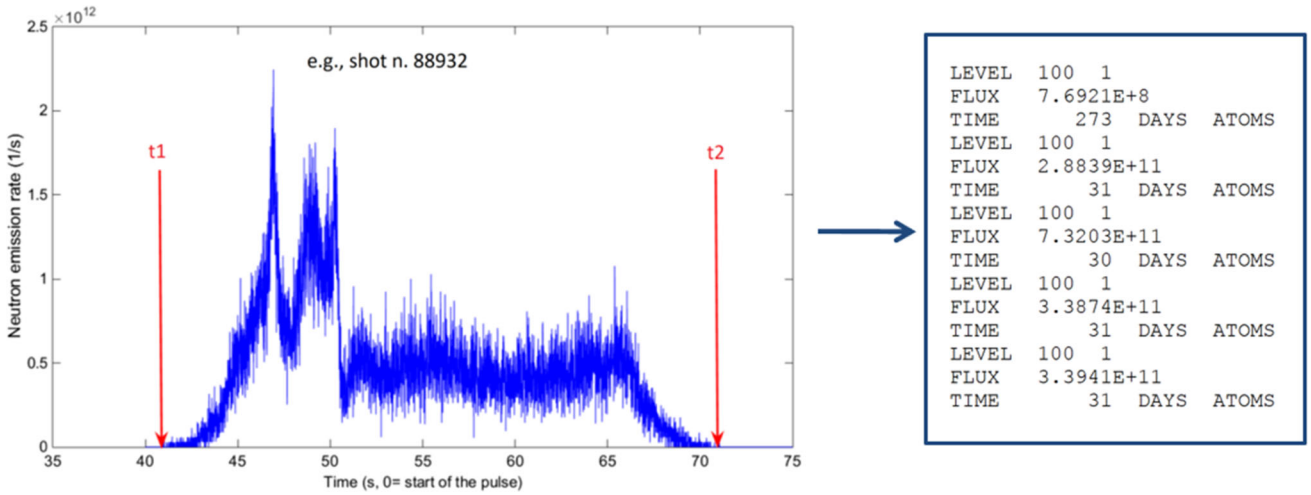

Fig. 6 Emission rate during a JET pulse as measured by KN1 on the left and piece of irradiation hystory in the FISPACT syntax on the right

coming from earlier campaigns is considered much less relevant and for this reason omitted in this preliminary assessment. Moreover, even the contribution coming from DD neutrons during DTE2 is neglected. The irradiation of JET across DTE2 is conveniently divided into some equivalent irradiation periods with a constant neutron emission rate averaged over their time duration, i.e., day-by-day irradiation periods from the beginning of the campaign up to two days before the end of the campaign and pulse-by-pulse neutron emission during the last two days. A dedicated computer routine was employed to create the irradiation history from the neutron emission rate measured by the JET neuton monitor KN1 across each plasma pulse of the campaign. The neutron yield of each pulse is calculated through integration of emission rate of each pulse. Pulses are then grouped to form the equivalent irradiation periods with a convenient temporal resolution. As an example, in Fig. 6, neutron emission rate is shown for a generic pulse and on the right a piece of irradiation hystory in the FISPACT syntax as produced by the computer routine.

Two irradiation histories are created to simulate the neutron activation at the end of plasma operation on November 6th and at the end of the DTE2 campaign on December 21th. Some short cooling times are selected for the comparison (3 and 12 h) and some longer time intervals (1, 7 and 12 days) from the end of neutron emission of the day. In addition, SDR is calculated at the locations of the ICs in octant 1 even after 29 days. In this case, the low intensity pulses occurred in the second part of January 2022, see upper plot of Fig. 4b, are discarded in the neutron activation calculation since considered negligible. SDR predictions and their ratio to the experimental values (C/E) are reported in Table 5. Uncertainty on C/E accounts for the experimental uncertainty on the SDR measurement, statistical error on the calculation and the uncertainty on the measurement of the neutron yield from KN1.

Table 5 Preliminary SDR calculations (*C*) with advanced D1S and comparison against measurements (*E*) as *C*/*E* ratio

Cooling time	IC Oct1 small		IC Oct1 big		IC Oct2 big	
	SDR (μGy/h)	*C*/*E*	SDR (μGy/h)	*C*/*E*	SDR (μGy/h)	*C*/*E*
Nov 6th 2021						
3 h	3146.9	0.94 ± 0.16	2830.9	0.96 ± 0.11	459.0	0.70 ± 0.08
12 h	1129.4	1.22 ± 0.29	1049.8	1.25 ± 0.15	87.1	0.57 ± 0.07
1d	686.5	1.35 ± 0.32	685.2	1.37 ± 0.17	32.8	0.48 ± 0.07
7d	228.0	1.47 ± 0.24	269.0	1.31 ± 0.15	3.8	0.59 ± 0.08
12d	212.0	1.52 ± 0.25	247.8	1.31 ± 0.15	4.3	0.68 ± 0.10
Dec 21st 2021						
3 h	7472.1	0.97 ± 0.18	6789.8	1.02 ± 0.12	1001.5	–
12 h	3398.1	1.26 ± 0.30	3236.9	1.36 ± 0.17	255.1	–
1d	2260.0	1.38 ± 0.31	2309.6	1.51 ± 0.18	109.8	–
7d	719.7	1.38 ± 0.23	848.9	1.40 ± 0.16	20.5	–
12d	668.7	1.42 ± 0.23	781.0	1.40 ± 0.16	18.6	–
29d	562.7	1.46 ± 0.24	658.1	1.40 ± 0.16	15.8	–

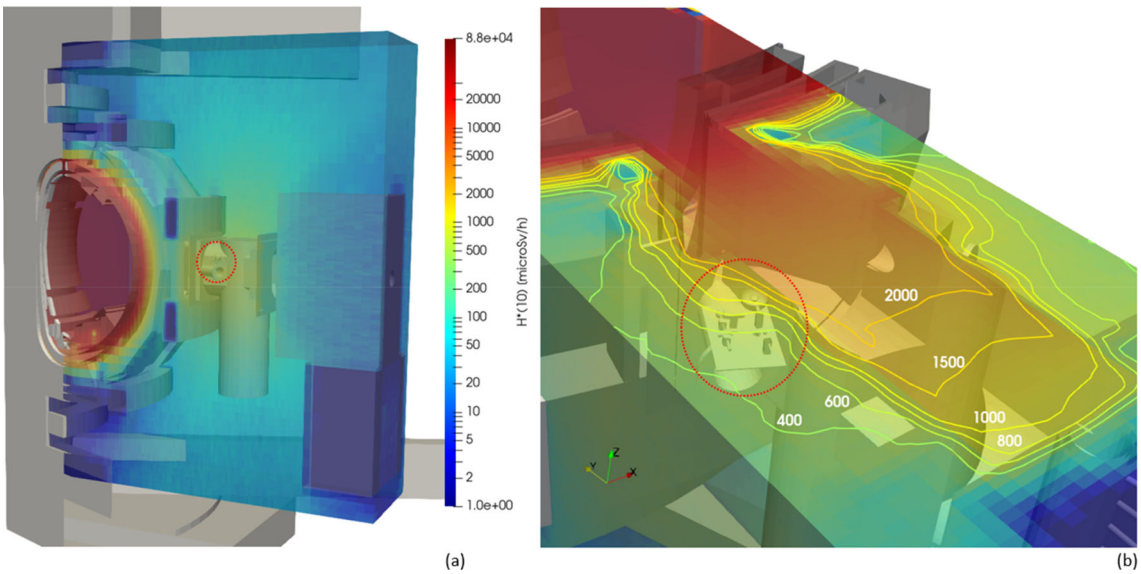

Fig. 7 SDR map of JET octant 1 12 days after shutdown: isometric view of the sector (**a**) and horizontal cross section in correspondence of the detector's shelf (**b**). Red circle indicates the location of the shelf in both

In octant 1 *C*/*E* is close to 1 within few hours, then a general trend of increasing overestimation is observed at longer cooling times upto ~ 50% for both ICsThe higher SDR at the location of the big IC in octant 1, with respect to the small IC, more visible at longer cooling times after shutdown, is confirmed also by measurements and it can be explained as it is more exposed to the radiation field coming from the plasma chamber through the equatorial port opening than the smaller IC. On the contrary, the SDR is underestimated in octant 2, up to ~ 50%. Among the sources of the discrepancy there is certainly the inaccuracy of the geometry model of JET, the incomplete knowledge of material impurities and the approximations introduced in the description of the neutron irradiation history. In facts, to limit the computation time, the neutron irradiation is approximated as continuous daily at an equivalent emission rate except for the last two days of DTE2, when neutron emission is modeled pulse by pulse. Moreover and in lack of more accurate information from other diagnostics not available at the time of performing this preliminary assessment, the fraction of neutrons at 14 MeV (produced by deuterium–tritium reactions) is considered constant and equal to the total neutron emission measured by KN1 during the campaign. A more accurate irradiation history will be created on the basis of the careful analysis of the neutron diagnostics data to determine the real 2.5 MeV neutron fraction coming from deuterium-deuterium reactions. Sources of discrepancy will be investigated further in relation to the major contributors to the SDRand nuclear data associated to them. In octant 1, Mn56 and Na24 are relevant at the short cooling times, i.e., up to 1 day, Ni57 up to few days, while Co58 becomes increasingly predominant at the longer cooling times from 1 to 29 days. In octant 2 another relevant gamma emitter is Cu64, of particular relevance in the first days after shutdown.

In Fig. 7 an isometric view of octant 1 with the SDR 3D map (a) and a horizontal cross section at the height of the shelf housing the two ICs (b) 12 days after shutdown are shown. The maps refer to the gamma ambient dose equivalent H*(10) [33] (the operational quantity for assessing effective dose in area monitoring). Contour lines indicate a spatial range of 2 mSv/h to 0.4 mSv/h in the area where the two ICs are located and it is evident the contribution coming from the equatorial port opening in the definition of the ex-vessel radiation field.

5 Conclusions and future work

The dosimetry system installed in the JET Torus Hall has provided a large set of data for code benchmarking of SDR tools employed for ITER since 2016, during DD, TT and the last DTE2 campaign. The less intense campaigns of the past (DD and TT) were employed also to test, to improve and to adapt the system to the operating conditions expected during DTE2, both hardware and software. The significant neutron fusion power produced during DTE2, allowed to reach dose rate level of interest for ITER. In particular, the intervals measured in octant 1, i.e., about 100 μGy/h to 20 mGy/h, and in octant 2, i.e., about 4 μGy/h to about 1 mGy/h, are relevant both for ITER interspaces and port cells SDR analyzes.

Measurements were analyzed following dosimetry protocols (IAEA and AAPM), accounting for deviations of measuring conditions with respect to the calibration laboratory and influence quantities which affect instrument reading. Experimental uncertainties related to the SDR measurement were evaluated as 3.0%, 3.9%, 4.2%, respectively for dosimeters based on the small and big ICs in octant 1 and the big IC in octant 2. PDF of air kerma rate is close to a Gaussian, the confidence probability associated to the standard deviation being equal to 66, 64 and 66%, respectively.

A thorough benchmark of SDR tools against experimental data is planned in the near future, on the base of a selection of experimental points from SDR measurements here presented and inputs prepared for radiation transport simulation with MCNP and neutron activation calculations with FISPACT codes.

Acknowledgements This work has been carried out within the framework of the EUROfusion Consortium, funded by the European Union via the Euratom Research and Training Program (Grant Agreement No 101052200—EUROfusion). Views and opinions expressed are however those of the author(s) only and do not necessarily reflect those of the European Union or the European Commission. Neither the European Union nor the European Commission can be held responsible for them.

Funding Open access funding provided by Ente per le Nuove Tecnologie, l'Energia e l'Ambiente within the CRUI-CARE Agreement.

Data Availability Statement The manuscript has associated data in a data repository. [Authors' comment: The datasets generated during and/or analyzed during the current study are available from the corresponding author on reasonable request].

References

1. J. Mailloux et al., Overview of JET results for optimising ITER operation. Nucl. Fusion **62**, 042026 (2022). https://doi.org/10.1088/1741-4326/ac47b4
2. P. Batistoni et al., Technological exploitation of deuterium–tritium operations at JET in support of ITER design, operation and safety. Fus. Eng. Des. **109–111**, 278–285 (2016)
3. P. Batistoni et al., Overview of neutron measurements in JET fusion device. Radiat. Prot. Dosimetry **180**(1–4), 102–108 (2018). https://doi.org/10.1093/rpd/ncx174
4. R. Villari et al., Neutronics experiments and analyses in preparation of DT operations at JET. Fusion Eng. Des. **109**, 895–905 (2016)
5. R. Villari et al., ITER oriented neutronics benchmark experiments on neutron streaming and shutdown dose rate at JET. Fusion Eng. Des.Des. **123**, 171–176 (2017). https://doi.org/10.1016/j.fusengdes.2017.03.037
6. MCNP X-5 Monte Carlo Team, MCNP—A General Monte Carlo N-Particle Transport Code Overview and Theory (Version 5, vol. I), Los Alamos National Laboratory, Report LA-UR-03-1987, 24 April 2003 (Revised 3.10.05)
7. R.A. Forrest, FISPACT 2007: User Manual, UKAEA, Fusion, Report UKAEA FUS 534 (2007)
8. D. Valenza et al., Proposal of shutdown dose estimation method by Monte Carlo code. Fusion Eng. Des. **55**, 411–418 (2001)
9. L. Petrizzi, et al., Improvement and benchmarking of the new shutdown dose estimation method by Monte Carlo code, Advanced Monte Carlo for Radiation Physics, Particle Transport Simulation and Applications, in *Proceedings of the MC2000 Conference 23–26 Oct. 2000 Lisbon, Portugal*. Springer (Feb 20010, pp. 865–870
10. R. Villari et al., Shutdown dose rate benchmark experiment at JET to validate the three-dimensional advanced-D1S method. Fusion Eng. Des. **87**, 1095–1100 (2012)
11. R. Villari et al., Shutdown dose rate assessment with the advanced D1S method: development, applications and validation. Fusion Eng. Des. **89**, 2083–2087 (2014)

12. Y. Chen, U. Fischer, Rigorous MCNP based shutdown dose rate calculations: computational scheme, verification calculations and applications to ITER. Fusion Eng. Des. **63–64**, 107–114 (2002)
13. N. Fonnesu et al., The preparation of the shutdown dose rate experiment for the next JET deuterium–tritium campaign. Fusion Eng. Des. **123**, 1039–1043 (2017). https://doi.org/10.1016/j.fusengdes.2017.01.030
14. N. Fonnesu et al., Shutdown dose rate measurements after the 2016 Deuterium-Deuterium campaign at JET. Fusion Eng. Des. **136**(Part B), 1348–1353 (2018)
15. N. Fonnesu et al., Shutdown dose rate studies for the DTE2 campaign at JET. Fusion Eng. Des. (2020). https://doi.org/10.1016/j.fusengdes.2020.112009
16. N. Fonnesu et al., Dose rate measurements during the tritium campaign at JET and diagnostic improvements for the deuterium–tritium experiments. IEEE Trans. Plasma Sci. **50**(11), 4131–4137 (2022). https://doi.org/10.1109/TPS.2022.3169631
17. International Commission on Radiation Units and Measurements (ICRU), Fundamental quantities and units for ionizing radiation, Journal of the ICRU 11 No 1 (2011) Report 85
18. PTW Freiburgh GmbH. 2023. https://www.ptwdosimetry.com/en/. Accessed 16 May 2023
19. International Atomic Energy Agency (IAEA), *Absorbed Dose Determination in External Beam Radiotherapy: An International Code of Practice for Dosimetry based on Standards of Absorbed Dose to Water, Technical Reports Series No. 398*, IAEA, Vienna (2000).
20. American Association of Physicists in Medicine (AAPM), AAPM's TG-51 protocol for clinical reference dosimetry of high-energy photon and electron beams. Med. Phys. **26**(9), 1847–1870 (1999)
21. The Italian National Institute of Ionizing Radiation Metrology (ENEA-INMRI). http://www.inmri.enea.it, 2023. Accessed 22 May 23
22. International Organization for Standardization (ISO), X and gamma reference radiation for calibrating dosemeters and doserate meters and for determining their response as a function of photon Energy, ISO 4037 (2009)
23. D.W.O. Rogers, C.K. Ross, The role of humidity and other correction factors in the AAPM TG-21 dosimetry protocol, Med. Phys. 15 (1) (1988)
24. O.A. Alduchov, R.E. Eskridge, Improved Magnus' form approximation of saturation vapor pressure. J. Appl. Meteor. **601–609**(35), 1996 (2016)
25. Guide to the Expression of Uncertainty in Measurement, *Standard ISO/IEC Guide 98–3* (International Organization for Standardization (ISO), Geneva, 2008)
26. Evaluation of Measurement Data – Supplement 1 to the Guide to the Expression of Uncertainty in Measurement – Propagation of Distributions Using a Monte Carlo Method, ISO/IEC Guide 98-3-1, International Organization for Standardization (ISO), Geneva, 2008
27. W.H. Press et al., *Numerical Recipes in FORTRAN. The Art of Scientific Computing* (Cambridge University Press, New York, 1993)
28. R. Villari et al., Development of the Advanced D1S for Shutdown Dose Rate Calculations in Fusion Reactors. Trans. Am. Nucl. Soc. **116**, 255–258 (2017)
29. G. Mariano et al., Progress in development of advanced D1S dynamic code for three-dimensional shutdown dose rate calculations. Fusion Eng. Des. 157, Article number 111631 (2020). https://doi.org/10.1016/j.fusengdes.2020.111631
30. R. Villari, D. Flammini, D17 - Final Version of MCNP Input for Shutdown Dose Rate Experiment, EUROfusion Report, IDM reference: EFDA_D_2MMSQ5 v1.0 (2018)
31. FENDL-3.1d: Fusion Evaluated Nuclear Data Library Ver.3.1d, January 2018
32. Ansys Space Claim, 2019 R1, ANSYS, Inc.
33. Y. Wu, J. Song, H. Zheng, G. Sun, L. Hao, P. Long, L. Hu, CAD-based Monte Carlo program for integrated simulation of nuclear system SuperMC. Ann. Nucl. Energy (2015). https://doi.org/10.1016/j.anucene.2014.08.058
34. T. Vasilopoulou et al., Activation foil measurmentes at JET in preparation for D-T plasma operation. Fusion Eng. Des. **146**, 250–255 (2019)
35. International Commission on Radiation Units and Measurements (ICRU), Quantities and Units in Radiation Protection Dosimetry, ICRU Rep. 51, Bethesda, MD (1993)